

Robust Implementation of Retrieval-Augmented Generation on Edge-based Computing-in-Memory Architectures

Ruiyang Qin¹, Zheyu Yan¹, Dewen Zeng¹, Zhengeng Jia¹, Dancheng Liu², Jianbo Liu¹, Ahmed Abbasi¹, Zhi Zheng¹, Ningyuan Cao¹, Kai Ni¹, Jinjun Xiong², Yiyu Shi¹
¹University of Notre Dame ²University at Buffalo–SUNY

ABSTRACT

Large Language Models (LLMs) deployed on edge devices learn through fine-tuning and updating a certain portion of their parameters. Although such learning methods can be optimized to reduce resource utilization, the overall required resources remain a heavy burden on edge devices. Instead, Retrieval-Augmented Generation (RAG), a resource-efficient LLM learning method, can improve the quality of the LLM-generated content without updating model parameters. However, the RAG-based LLM may involve repetitive searches on the profile data in every user-LLM interaction. This search can lead to significant latency along with the accumulation of user data. Conventional efforts to decrease latency result in restricting the size of saved user data, thus reducing the scalability of RAG as user data continuously grows. It remains an open question: how to free RAG from the constraints of latency and scalability on edge devices? In this paper, we propose a novel framework to accelerate RAG via Computing-in-Memory (CiM) architectures. It accelerates matrix multiplications by performing in-situ computation inside the memory while avoiding the expensive data transfer between the computing unit and memory. Our framework, **Robust CiM-backed RAG (RoCR)**, utilizing a novel contrastive learning-based training method and noise-aware training, can enable RAG to efficiently search profile data with CiM. To the best of our knowledge, this is the first work utilizing CiM to accelerate RAG.

1 INTRODUCTION

The emerging Large Language Models (LLMs) are deployed primarily on centralized cloud platforms [1, 2] (Cloud LLMs), raising concerns about user privacy and trustworthy issues [3]. These issues become even more prominent in areas such as healthcare [4], companionship [5], and personal assistance [6], where the user privacy and trustworthiness of LLMs are crucial. To address these issues, the cloud LLMs will eventually transform into personalized LLMs, capable of generating personalized responses, deployed on edge devices (Edge LLMs), where users can keep all their private data and the model learns from those data locally.

To better suit the needs of individual users, Edge LLMs must learn from user interactions. However, their capability of learning is constrained by their limited RAM and computational power. Similar to Cloud LLMs, the Edge LLMs primarily learn by fine-tuning their model parameters. Yet, given that these models often contain over 3 billion parameters, updates can be challenging, even with numerous efforts to accelerate them [7–9]. For example, using the experimental high-performance embedded system like NVIDIA-AGX, the pockengine method [9] can still take 90 hours to learn from a middle-sized dataset Alpaca with only 52k documents, making this option impractical for normal users.

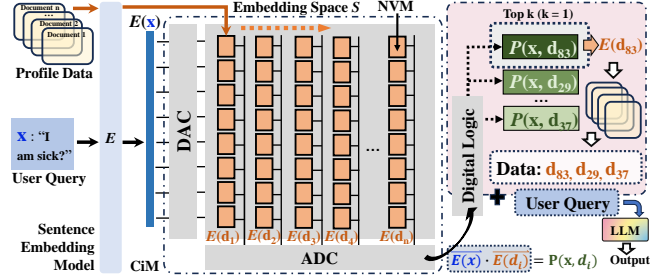


Figure 1: The workflow of RAG on edge-based CiM. CiM performs max inner product search (MIPS) to retrieve the top-ranked documents, concatenating them with user query to allow the LLM to generate personalized responses.

Retrieval-augmented generation (RAG), on the other hand, is a more resource-efficient choice [10], and hence becoming the de facto learning method for Edge LLMs. In a typical RAG system, it consists of a retriever and a generator. The retriever is commonly backed by max inner product search (MIPS). When the retriever receives a user query, it will retrieve the most relevant document from profile data, as shown in Figure 1. The profile data has many documents, and each document d_i contains specific information that may be relevant to user queries. The generator can be seen as a LLM, which takes the user query x and retriever-obtained documents as a prompt and generates a corresponding response. For every document d_i and the user query x , RAG utilizes a sentence embedding model shown in Figure 1 to convert them into vectors (i.e., $E(d_i)$ and $E(x)$, respectively). The vectors for documents can be named as document embeddings and stored as a matrix as shown in Figure 1. The vector for user query, named query embedding $E(x)$, will be used in MIPS to perform inner product with every document embedding. The larger the product $P(x, d_i)$, the more semantic similar it will be between the user query and the document.

Using RAG, Edge LLMs can provide user-preferred responses by retrieving relevant documents from profile data, and the profile data can be incrementally updated with new documents. This is an efficient learning process without costly updating the model parameters via fine-tuning [11]. Other than the inevitable LLM inference cost, the primary computational cost of RAG is about retrieval, which is more than ten times less than the cost of updating model parameters.

While the computational cost of RAG is more edge-friendly, there still exist two issues impeding RAG from being deployed for real-time user interaction on Edge LLMs. Firstly, the growing profile data as stored cannot be unlimited without affecting the access time. If the size of the profile data exceeds the RAM capacity,

it will need to be offloaded into the storage, such as a hard disk drive (HDD) or solid-state drive (SSD). Accessing data from HDD or SSD will significantly increase the data transfer latency [12], rendering real-time user interaction impractical. Secondly, the core retrieval method of RAG, MIPS, may experience decreased efficiency as profile data grows, and it can become potentially prohibitive when dealing with overwhelmingly large datasets. For example, on Raspberry Pi 4B, MIPS can take 5 minutes to find one appropriate profile data among 21M documents [10], which is even longer than the 2-minute inference time of an Edge LLM. Unfortunately, few efforts have been made to optimize RAG towards Edge LLMs.

Thus, we propose to utilize the Computing-in-Memory (CiM) architecture to address this issue. As shown in Figure 1, CiM architectures using memory arrays have shown substantial promise in accelerating matrix-vector multiplication [13], which is the key operation of MIPS. The CiM architectures often utilize massive parallel processing to perform computations directly within the memory array where the data is stored, such that they can minimize the data movement through in-situ data access and significantly increase the throughput [14]. Given the same amount of documents, CiM can finish computation within 50ms [15], which is negligible compared to the computation latency on normal edge devices. Furthermore, by incorporating non-volatile memory (NVM) devices, such as phase-change memories (PCMs), resistive random-access memories (RRAMs), and ferroelectric field-effect transistors (FeFETs), CiM can outperform conventional MOSFET-based designs in terms of energy efficiency [16].

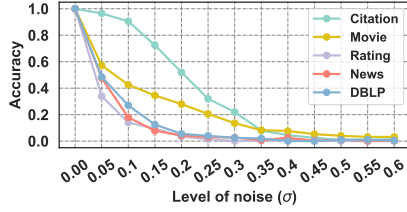


Figure 2: The impact on MIPS accuracy when the RAG’s document embedding is perturbed by various levels of Gaussian noise caused by the device variations. An accurate retrieval means the document retrieved under the impact of the noise is the same as that retrieved without noise.

Unfortunately, simply changing the underlying hardware is not enough, as the non-idealities of the NVM devices in CiM array could greatly deteriorate the RAG performance. First, the operations performed in CiM architectures are susceptible to various sources of noise, including electronic noise (thermal, shot, and flicker), device-to-device variability, and line noise from the supporting circuitry [17]. These noise sources can corrupt the computations, especially when the signal levels are close to the noise floor, which is a common scenario in high-precision tasks. Such noise issues are critical in RAG applications where the accuracy and quality of the generated content heavily rely on the precision of the underlying computations. Additionally, the CiM architecture is primarily designed and optimized for low-resolution computation [18]. Moreover, CiM arrays are typically sized at a fixed dimension, such as 64x64 [19],

which is different from the documents’ embedding dimension (*e.g.*, 128). Therefore, both RAG’s data precision (typically FP32) and its embedding dimension need to be reduced to fit in the size of CiM’s crossbar arrays. To illustrate the impact of these on RAG, as an example, we present a preliminary study on MIPS performance in Figure 2, where we use a simple yet representative Gaussian noise to simulate the noise from the device variations in CiM. As shown in Figure 2, as the noise level increases, MIPS accuracy (specified in section 4.1.3) drops dramatically, approaching random guessing.

To address these issues, we further propose a novel optimization framework for CiM-backed RAG, called **Robust CiM-backed RAG (RoCR)**. The framework consists of three parts. The first part is a contrastive learning method. We use it to optimize the document embedding model. The second part is a novel data construction method to generate both positively and negatively labeled data pairs for contrastive learning. For the profile data, they can be either labeled to indicate the explicit user-preferred response to certain input, or simply statements without explicit labels that only implicitly indicate user preferences. Our data construction method is capable of dealing with both types of profile data. The third part is a noise-aware training method. It goes in tandem with contrastive learning to obtain a sentence embedding model that can generate document and user query embeddings with high noise-resilient capability, while such embeddings can fit into CiM architectures under different designs and configurations.

Our major contributions can be summarized as:

- We propose the first work to harvest CiM advantages for RAG acceleration on the edge. We provide a pathway to utilize emerging CiM devices to expand the Edge LLMs’ capability in terms of storing a high volume of profile data with fast MIPS computing.
- We introduce noise-aware training to enhance the noise-resilient capabilities of RAG’s document embedding. The resulting noise-resilient embeddings can be reused robustly, saving resources needed to calibrate and regenerate embeddings.
- Our experiments on various datasets show that our proposed framework can improve the RAG performance on multiple CiM devices up to 35%, approaching to the theoretical RAG performance. Across a wide device variation (noise) range on a single CiM device, our proposed framework can still improve the RAG performance.

2 RELATED WORK

2.1 CiM Architectures and their NVMs

As shown in the middle part of Figure 1, memory arrays are the key component for vector-matrix multiplication. In this array, matrix values are stored at NVM cells, such as emerging NVM technologies like PCMs, RRAMs, and FeFETs, at the cross-points of vertical and horizontal lines. Simultaneously, vector values flow along the horizontal lines of the array. Operations within the memory array take place in the analog domain by exploiting law of physics directly. However, for other essential functions like shift-and-add for multiple bits and sorting to find the top-k ranked values would be done in the digital domain. Thus, digital-to-analog and analog-to-digital

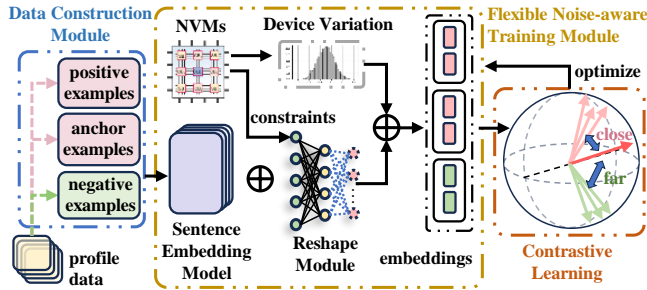


Figure 3: Overview of the proposed Robust CiM-backed RAG framework (RoCR). It optimizes the sentence embedding model to adapt different types of NVMs utilized by CiM.

converters (DACs and ADCs) are used to connect these different components.

CiM arrays suffer from various sources of variations and noises. Two major ones include spatial variations and temporal variations. Spatial variations result from fabrication defects and have both local and global correlations. FeFET devices also suffer from temporal variations due to the stochasticity in memory switching and also aging, which causes fluctuations in conductance when programmed at different times. Temporal variations are typically independent from device to device and are irrelevant to the value to be programmed [20]. In this work, as a proof of concept, we focus on the impact of temporal variations in the programming process on DNN performance. Temporal variation makes the programmed resistance of a device deviate from what is expected. The proposed framework can also be extended to other sources of variations with modification.

Measurement results [21, 22] show that the noise on DNN weights caused by device variations can be safely modeled as a Gaussian noise with zero mean, each with a standard deviation associated with the weight value. A detailed representation is given by:

$$\mathbf{v} = \mathbf{v}_0 + \Delta\mathbf{v}, \Delta\mathbf{v} \sim \mathcal{N}(0, \sigma_v) \quad (1)$$

where \mathbf{v} is the actual embedding deployed on the accelerators, \mathbf{v}_0 is the target embedding value, and σ_v is a value measured by the experiments. We collect the measurement results from RRAM and FeFET devices and the specific value will be discussed in Section 4.1.

2.2 Past Noise Mitigation Methods

Several strategies have been introduced to tackle the challenge of device variations in CiM accelerators. These methods can be separated into software and hardware-based techniques.

The software-based techniques are generally developed to obtain more robust DNN models [19, 22–24] or recommendation systems [25], and are thus not suitable for generating more robust MIPS solutions.

For the hardware techniques, the write-verify procedure [26, 27] is one of the most commonly used approach during programming. Initially, a NVM device is programmed to a set state via a designated pulse pattern. Subsequent to this, the device’s value is verified to ascertain if its conductance aligns with a stipulated range of the desired value, essentially assessing its accuracy. If discrepancies

arise, a supplemental update pulse is initiated to reset the device conductance nearer to the target. This loop persists until the disparity between the programmed device value and the target value diminishes to a satisfactory margin, typically taking a handful of cycles. Cutting-edge research suggests that by selectively applying write-verify to a subset of pivotal devices, one can uphold the average accuracy of a DNN [21]. Additionally, a variety of circuit design initiatives [18, 28] have been put forth to counteract device variations.

3 PROPOSED WORK

3.1 Framework Overview

As shown in Figure 3, our proposed framework, **Robust CiM-backed RAG (RoCR)**, consists of three stages. First, we apply contrastive learning to utilize the training data to optimize the training module. To do that, in the second stage, we take the profile data and construct via a data construction module to obtain contrastive training data pairs, which are then used in the flexible noise-aware training module. In the third stage, we obtain the constraints of NVMs in CiM via profiling. These constraints will be encoded into the flexible noise-aware training module and used to train the sentence embedding model so that it can generate embedding that are robust against device variation of the target NVMs. After training, the training module can be turned into a new sentence embedding model and generate CiM-friendly embeddings.

3.2 Contrastive Learning: Triplet Loss Function

When we apply RAG using CiM, we first need to store embeddings into NVMs as shown in Figure 1. Such embeddings are generated by the sentence embedding model, and they are the numerical representations of profile data. Each single document in the profile data can have its unique embedding, which is a vector. The embeddings stored on NVMs can consist of a matrix as the orange blocks shown in Figure 1. Given a user query, which will also be converted into an embedding, CiM can operate MIPS between this user query embedding and all profile embeddings simultaneously via vector-matrix multiplication. The top-ranked values in the product will be used as the index to retrieve the corresponding document data, as the pink block shown in Figure 1. This retrieved user-relevant document is the output of MIPS.

However, as we have explained in Section 2.1, writing the document embeddings into NVMs can cause them to suffer from temporal variations (device variations). Then, the NVM-stored embeddings will be different from the original sentence embedding model generated embeddings. As shown in Figure 4, the vanilla embedding model generates desired embedding, which will deviate to the noise embedding under device variation, such that the irrelevant embedding is ranked higher than desired embedding due to its larger inner product.

Contrastive learning can learn the representations via push away dissimilar examples and pull close similar examples [29]. In particular, the contrastive loss function can be used to increase the distance between dissimilar examples.

In our work, we propose to improve the noise-resilient capability by contrastive learning. By increasing the distance between

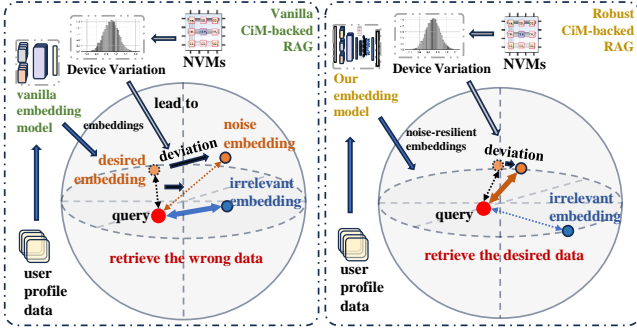


Figure 4: Improvement by our Robust CiM-backed RAG. Our framework generates noise-resilient embeddings, as shown the orange and blue point in right subfigure

dissimilar examples, as shown the right subfigure in Figure 4, deviated desired embedding will still have a larger inner product with the query compared to the irrelevant embedding. Our contrastive learning loss function is based on Weinberger et al. [30]. For each example x_i in a mini-batch of N anchor examples, our data construction method will construct K positive and K negative examples corresponding to x_i . We can have $\{(x_i, x_i^-, x_i^+)_{k=1, \dots, N}\}_{k=1, \dots, K}$, in which x_i^- and x_i^+ are negative and positive examples corresponding to x_i , where x_i is closer to x_i^+ compared to x_i^- . Also, $emb(x_i)$ represents the learned embedding of x_i . Then the loss function \mathcal{L} can be defined as:

$$\mathcal{L} = \sum_{i=1}^N \frac{1}{K} \sum_{k=1}^K \max \left(0, d(x_i, x_{i(k)}^-) - d(x_i, x_{i(k)}^+) + m \right), \quad (2)$$

$$d(x_a, x_b) = \text{sim}(emb(x_a), emb(x_b))$$

The distance $d(x_a, x_b)$ is calculated by the Euclidean distance between embeddings of two data $emb(x_a)$ and $emb(x_b)$. The function $\text{sim}()$ calculate the semantic similarity.

3.3 Data Construction

To train the sentence embedding model via contrastive learning, it is critical to construct pairs of examples where the positive examples and negative examples need to be distinct from each other [31]. In our work, since we use triplet contrastive loss, instead of pairs of examples, we will construct trios of examples where each triplet contains an anchor, positive, and negative example.

We use profile data to construct triplets of examples. For the profile data, it is generated by the user during the user-LLM interaction and contains the user preference information. There exists two situations for such data. First, the profile data can contain explicit labels indicating the user preferred response to the corresponding content. Second, the profile data also can be statements containing the user-related information but without explicit user preferences. As shown in Figure 5, to deal with the two situations, we come up with two data construction methods: Construction Data with Explicit labels (CDE) and Construction Data with Implicit labels (CDI).

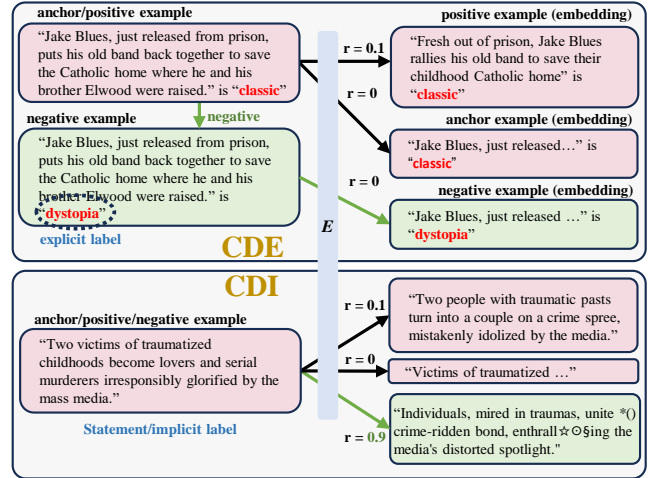


Figure 5: Examples of the two data construction methods. For data with explicit labels, CDE is used to construct the training data. For data without explicit labels (implicit labeled data), CDI is used to construct the training data.

3.3.1 Construction Trios via Data with Explicit Labels (CDE).

For the data with explicit labels, each of the data consists of a textual content c and its corresponding label l which indicates the user preferred response regarding to the content c . As shown in the CDE part in Figure 5, there exists explicit label circled by dashed line. Using the profile data, we will construct triplet examples in the format of (x_i, x_i^-, x_i^+) . Given a dataset \mathcal{D} with size of n profile documents, each piece of data consists of a content c_i and the corresponding label l_i where $i \in \{1, 2, \dots, n\}$. The anchor example x_i can be constructed as:

$$x_i = c_i \oplus l_i, \quad \text{for } i = 1, 2, \dots, n \quad (3)$$

where \oplus denotes a concatenation operation, specifically used here to combine label and content. Negative examples x_i^- can be constructed by concatenating c_i with a random label l_j that is different from l_i as follows:

$$x_i^- = c_i \oplus l_j, \quad \text{where } l_i \neq l_j. \quad (4)$$

Randomly assigning a different label ensures diversity in the negative examples while maintaining the same content from the anchor.

Different from constructing anchor and its negative examples, it is challenging to construct positive examples corresponding to the anchor examples since it is more difficult to formalize semantically similar data than to formalize semantically dissimilar data. To construct positive examples, we follow the SimCSE method [32] to add a dropout rate r into the sentence embedding model \mathcal{M} . The process for constructing positive examples involves two main steps.

First, the textual positive example is formalized as:

$$x_i^+ = x_i, \quad \text{for } i = 1, 2, \dots, n \quad (5)$$

where we align each anchor with the corresponding positive example. This step effectively duplicates the anchor data as a starting point for generating the embeddings.

Second, the embedding generation process varies based on the dropout rate applied within the model \mathcal{M} . When model \mathcal{M} is utilized to generate embeddings for anchor and negative examples, the dropout rate is set to 0. In contrast, for generating embeddings for positive examples, a non-zero dropout rate r is used. The anchor, negative, positive examples, as shown in Figure 5, can be constructed as:

$$\begin{aligned} \text{emb}(x_i) &= \mathcal{M}(x_i, \text{dropout} = 0) \\ \text{emb}(x_i^-) &= \mathcal{M}(x_i^-, \text{dropout} = 0) \\ \text{emb}(x_i^+) &= \mathcal{M}(x_i^+, \text{dropout} = r) \end{aligned} \quad (6)$$

The condition of $r \neq 0$ can induce variation in the embeddings, enhancing the model's ability to recognize semantically similar yet variably expressed content.

Given the construction factor K , we can construct the triplet data examples as:

$$\mathcal{D}_{\text{triplet}} = \bigcup_{i=1}^N \left\{ (x_{i(k)}, x_{i(k)}^-, x_{i(k)}^+) : k = 1, 2, \dots, K \right\} \quad (7)$$

For the triplet data examples $\mathcal{D}_{\text{triplet}}$, their embeddings for each augmentation k are given by:

$$\mathcal{E} = \bigcup_{i=1}^N \left\{ (\text{emb}(x_{i(k)}), \text{emb}(x_{i(k)}^-), \text{emb}(x_{i(k)}^+)) : k = 1, 2, \dots, K \right\} \quad (8)$$

As shown in Figure 5, for data with explicit labels, a content c can concatenate with its corresponding label l to formalize the positive and anchor example. That content c can also concatenate with other labels l' to formalize the negative example. The positive example can be finally obtained from the sentence embedding model with dropout rate r . The anchor and negative example can be finally obtained from the sentence embedding model with $r = 0$.

3.3.2 Construction Trios via Data with Implicit Labels (CDI). For data with implicit labels, each of the data consists of solely textual content c . As shown of the CDI part in Figure 5, there is no explicit label to indicate user preferences. Instead, the data can be seen as a statement containing some user-related information. To construct the anchor examples and positive examples, we can use the exact same method in EDC. Given a dataset \mathcal{D} with size of n profile data, each piece of data consists of a content c_i . The anchor data x_i can be constructed as:

$$x_i = c_i, \quad \text{for } i = 1, 2, \dots, n \quad (9)$$

For each anchor data x_i , constructing its corresponding negative example is not as simple as merely concatenating the content c_i with a non-corresponding label l_k . To construct negative examples, we employ a reciprocal approach with the positive examples, applying a similar method to both.

We first initialize the negative example and positive example following the equation 5:

$$x_i^- = x_i^+ = x_i, \quad \text{for } i = 1, 2, \dots, n \quad (10)$$

For the positive example x_i^+ , it can be finalized by incorporating a dropout rate r into the sentence embedding model \mathcal{M} , where a

rate of $0 < r \leq 0.2$ can generate a sentence embedding with a semantic representation similar to x_i and ensure good model training performance [32]. Increasing the dropout rate to a higher value, such as 0.5, can distort the semantic representation of x_i^+ , making it dissimilar to that of x_i . Training the model with such positive examples can result in poorer performance. For positive examples in training the sentence embedding model, the higher dropout rate performs more like a noise rather than a data augmentation method.

In our work, we train the sentence embedding model to generate embeddings that maintain their integrity under noisy conditions, such as during writing into Compute-in-Memory (CiM). The noise can alter or fragment the original semantic representations. For instance, as illustrated in Figure 5, using a high dropout rate $r = 0.9$ can lead to a negative example with a corrupted representation. Although it may lack certain informative content, this negative example becomes semantically distinct from both the anchor and positive examples, effectively simulating the effect of CiM corruption. This approach not only differentiates the negative examples semantically but also aligns them with the corrupted data scenarios for noise-aware training.

Given the triple examples (x_i, x_i^-, x_i^+) , for $i = 1, 2, \dots, n$ as shown in equation 10, we have the dropout rate r for formalizing the positive examples where $0 < r \leq 0.2$. Correspondingly, the dropout rate for formalizing the negative examples can be $1 - r$. Given the sentence embedding model \mathcal{M} , the anchor example, positive example, and negative example can be constructed as:

$$\begin{aligned} \text{emb}(x_i) &= \mathcal{M}(x_i, \text{dropout} = 0) \\ \text{emb}(x_i^-) &= \mathcal{M}(x_i^-, \text{dropout} = 1 - r) \\ \text{emb}(x_i^+) &= \mathcal{M}(x_i^+, \text{dropout} = r) \end{aligned} \quad (11)$$

3.4 Flexible Noise-aware Training

In the previous two stages, we construct the data to train the sentence embedding model based on contrastive learning. Meanwhile, the training can be more effective when injecting the simulated device variation [33] so that the model can be optimized with consideration of the device variation. Additionally, the sentence embedding model needs to produce embeddings that can fit with the different CiMs, which might have various NVM designs. To do that, we need the sentence embedding model reshapes its output embeddings into certain dimensions and precision. Hence, we propose a flexible noise-aware training method, which can generate the noise-resilient embedding, fitting to various CiMs.

As shown in Figure 3, in the flexible noise-aware training module, the embedding generated by sentence embedding model will be shaped based on the CiM's NVMs constraints where required dimension is d and required precision is p , and being injected device variation to formalize the embeddings. The reshape module, shown in Figure 3, seen as an autoencoder to reconstruct its input embedding [34], can be expressed as $\text{shp}()$, initialized by d and p , takes the anchor embedding $\text{emb}(x_i)$ as input. We can have $\text{shp}(\text{emb}(x_i)) = \text{emb}(x_i)^{d \times p}$. Based on the device variation shown as Table 2, we can have:

$$\text{emb}(x_i)_{\sigma}^{d \times p} = (e' * L_0 + e' * L_1 + e' * L_2 + e' * L_3) * \sigma, \quad (12)$$

Table 1: Performance comparison between our framework and four baselines on five CiM devices with device variation specified in Table 2 across five datasets. Evaluate the performance of our framework using EDC (RoCR-EDC) and using IDC (RoCR-IDC) to optimize the performance of RAG, which utilizes Gemma-2 as its LLM.

Dataset		Citation		Movie		Rating		News		DBLP	
CiM	Method	Acc \uparrow	F1 \uparrow	Acc \uparrow	F1 \uparrow	MAE \downarrow	RMSE \downarrow	ROUGE-1 \uparrow	ROUGE-L \uparrow	ROUGE-1 \uparrow	ROUGE-L \uparrow
Device-1	SWV	0.4208	0.3339	0.1305	0.1974	0.3850	0.8093	0.0754	0.0731	0.1709	0.1590
	CxDNN	0.4223	0.3576	0.1516	0.1762	0.4404	0.9135	0.0640	0.0632	0.1646	0.1449
	CorrectNet	0.4155	0.3791	0.0996	0.1305	0.3609	0.7071	0.0512	0.0764	0.1603	0.1538
	Vanilla RAG	0.4401	0.3476	0.1017	0.0838	0.3903	0.8944	0.0754	0.0731	0.1731	0.1473
	RoCR-CDE	0.5536	0.3956	0.2242	0.2303	0.3108	0.6856	0.1041	0.0987	0.2066	0.1924
	RoCR-CDI	0.5409	0.5117	0.2273	0.2487	0.2767	0.6083	0.0831	0.0808	0.2317	0.2176
Device-2	SWV	0.1831	0.1552	0.1992	0.1957	0.4205	0.8775	0.0296	0.0289	0.1968	0.1874
	CxDNN	0.4013	0.3557	0.2167	0.2019	0.4423	0.8367	0.0604	0.0791	0.1517	0.1401
	CorrectNet	0.3827	0.3209	0.1625	0.1909	0.3762	0.8062	0.0513	0.0505	0.2042	0.1945
	Vanilla RAG	0.4801	0.3462	0.1576	0.2079	0.4153	0.9354	0.0296	0.0289	0.1618	0.1353
	RoCR-CDE	0.5407	0.4396	0.2924	0.2509	0.2553	0.5385	0.1209	0.0946	0.2025	0.1906
	RoCR-CDI	0.5299	0.4591	0.2971	0.2386	0.2124	0.5763	0.0884	0.0853	0.2240	0.2098
Device-3	SWV	0.2450	0.2564	0.1695	0.1641	0.3460	0.7416	0.0725	0.069	0.1018	0.0954
	CxDNN	0.4811	0.4006	0.2367	0.2113	0.2851	0.6928	0.0761	0.0707	0.1425	0.1111
	CorrectNet	0.4510	0.3918	0.0792	0.1029	0.3704	0.7937	0.0585	0.0555	0.1715	0.1346
	Vanilla RAG	0.4852	0.3618	0.1614	0.1636	0.3255	0.7649	0.0725	0.0690	0.1647	0.1437
	RoCR-CDE	0.5139	0.4116	0.2242	0.2215	0.3208	0.6481	0.0825	0.0805	0.1893	0.1754
	RoCR-CDI	0.5515	0.4984	0.2152	0.2131	0.2916	0.6245	0.1099	0.1049	0.2294	0.2140
Device-4	SWV	0.5135	0.4260	0.1271	0.1178	0.3610	0.8196	0.0259	0.0256	0.1871	0.1786
	CxDNN	0.4733	0.3964	0.1267	0.2158	0.3468	0.7616	0.0646	0.0634	0.1603	0.1538
	CorrectNet	0.4628	0.4019	0.1592	0.1847	0.4013	0.9274	0.0705	0.0750	0.1628	0.1292
	Vanilla RAG	0.2101	0.2401	0.1219	0.2019	0.4015	0.8544	0.0505	0.0489	0.1929	0.1814
	RoCR-CDE	0.5836	0.5555	0.1706	0.2817	0.3139	0.6856	0.0873	0.0851	0.1984	0.1882
	RoCR-CDI	0.5352	0.4289	0.1642	0.2445	0.2706	0.5916	0.1154	0.1128	0.2148	0.1978
Device-5	SWV	0.4320	0.3541	0.1250	0.1076	0.3652	0.7616	0.0434	0.0427	0.0985	0.0923
	CxDNN	0.4301	0.0538	0.0751	0.0458	0.3503	0.8185	0.0707	0.0682	0.2042	0.1945
	CorrectNet	0.4145	0.3926	0.1083	0.1395	0.5526	0.8185	0.0735	0.0776	0.2096	0.1879
	Vanilla RAG	0.4256	0.3522	0.0847	0.0863	0.3951	0.8515	0.0676	0.0653	0.2018	0.1846
	RoCR-CDE	0.5698	0.5223	0.2152	0.1669	0.2959	0.6245	0.0936	0.0891	0.1946	0.1844
	RoCR-CDI	0.5254	0.4504	0.2394	0.2458	0.2624	0.6325	0.0799	0.0764	0.2238	0.2095

where $e' = emb(x_i)^{d*P}$. The device variation, as noise, is injected into embeddings to formalize $emb(x_i)_{\sigma}^{d*P}$, which will be used in contrastive learning to train the sentence embedding model, as shown in Figure 3.

4 EXPERIMENTAL EVALUATION

4.1 Experimental Setup

4.1.1 Datasets. To demonstrate our robust CiM-backed RAG, we employ five datasets with different tasks and domains, including Citation Identification [35] (**Citation**), Movie Tagging [36] (**Movie**), Product Rating [37] (**Rating**), News Headline Generation [38] (**News**), and DBLP-Citation-network V14 [39] (**DBLP**) to evaluate the proposed framework. The data in each dataset consists of query data and profile data. In our evaluation, the profile data will be used to formalize user history, and the profile corresponding query data will be used as the user input. The first three datasets contain binary, five-class, and fifteen-class classification tasks respectively. The last two datasets contain text generation tasks. In the Citation Identification dataset, every piece of query data consists of a paper title and two references, and the correct reference is provided. RAG uses the profile data corresponding to the paper titles with their detailed contents to choose the appropriate reference. In the Movie Tagging dataset, each query data contains a description of a movie,

and RAG uses a similar description and its corresponding tag in the profile data to tag the query data. The Product Rating dataset has a similar structure as the Movie Tagging dataset. In News Headline Generation and DBLP datasets, each query data contains an abstract, which can be summarized into a title. RAG uses a similar abstract and its corresponding title in profile data to generate the title for query data. All five datasets have labels in their query data.

4.1.2 Default Experimental Setting. Our framework chooses *all-MiniLM-L6-v2* [40] as the sentence embedding model. For each dataset, we randomly select 2000 documents from profile data as the anchor examples. To examine the data construction method of CDE, we set the augmentation factor $k = 5$ to obtain 10000 negative and positive examples. We set dropout rate as 0.1 to obtain the positive examples while maintain it as 0 when process anchor and negative examples. To examine the data construction method CDI, we set dropout rate for positive examples as 0.1 and dropout rate for negative examples as 0.9. To align with experiments for CDE, we also set $k = 5$ in the experiments for CDI. For the experimental results, we run five times and get the average. In experiments, we set the device variation $\sigma = 0.1$ and shape embeddings into dimension of 64 with precision of *int8*. The learning rate is $2e - 5$.

In all experiments, we adhere to the device variation model previously described. The specific parameters are abstracted and then simplified from three representative NVM devices, two of them

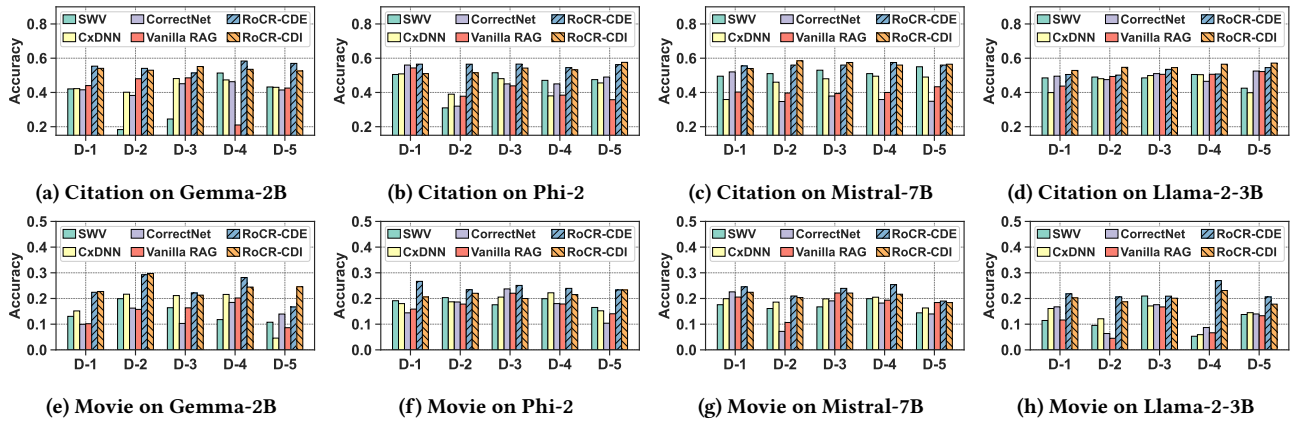


Figure 6: Performance comparison between our framework and four baselines on RAG utilizing the LLMs including Gemma-2B, Phi-2, Mistral-7B, and Llama-2-3B with device variation specified in Table 2, given dataset *Citation* and *Movie*.

Table 2: Device non-ideality modeling for different real and synthesized devices. For devices with more than two levels, the device variation for each level is depicted as L_x .

Name	# of Levels	Device Variations σ_o			
		L_0	L_1	L_2	L_3
$RRAM_1$ (Device-1)	1	0.0100	0.0100	0.0100	0.0100
$FeFET_2$ (Device-2)	4	0.0067	0.0135	0.0135	0.0067
$FeFET_3$ (Device-3)	4	0.0049	0.0146	0.0146	0.0049
$RRAM_4$ (Device-4)	4	0.0038	0.0151	0.0151	0.0038
$FeFET_6$ (Device-5)	4	0.0026	0.0155	0.0155	0.0026

are resistive random-access memory (RRAM) devices extracted from [27, 41] and the other is a ferroelectric field effect transistor (FeFET) device extracted from [42]. We name them $RRAM_1$, $RRAM_4$ and $FeFET_2$, respectively. We also extrapolate the modeling data to obtain two synthesized $FeFET_3$ and $FeFET_6$ devices. Detailed device modeling results are demonstrated in Table 2. A x -level device means this device can represent x distinct values and $\sigma_{L_2} = 0.01$ means the variation of this device is 0.01 when it is representing the level value 2. Using the device variations obtained from real CiM devices, we perform our experiments on a single Nvidia A10 GPU.

Document embeddings are shaped based on different CiM devices and stored as parallel arrays, similar to how they would be mapped to multiple NVM devices in practical scenarios. For example, if an embedding is shaped to contain all uint8 values, when it is mapped to 4-level (2-bit) devices such as $FeFET_2$, each element of the vector is represented by four devices.

4.1.3 Evaluation Methods. Our first three datasets examine the model classification capability, and the rest of two datasets examine the text generation capability. In particular, dataset *Citation* and *Movie* has two and fifteen labels respectively. We can examine the binary and multiclass classification capabilities of the LLMs enhanced by our framework. In this way, we use accuracy to examine the ability of the models to correctly classify instances across different classes, and we use F1 score to examine the balance between precision and recall in classification tasks. For dataset *Rating*, while

it has five labels and also examine the multiclass classification, we use mean absolute error (MAE) and root mean square error (RMSE) to evaluate from a regression perspective [43]. For MAE, it measures the average magnitude of errors in the predictions, providing a straightforward assessment of the model’s overall accuracy in predicting the rating values. For RMSE, it captures the square root of the average squared differences between predicted and actual ratings, offering a metric sensitive to larger errors, which can highlight significant discrepancies between the model’s predictions and true values. For dataset *News* and *DBLP*, their labels are sentences. Such datasets examine the text generation capabilities. We use ROUGE-1 and ROUGE-L to evaluate the overlap between generated texts and reference texts [44], capturing both the precision and recall of individual words (ROUGE-1) and the longest matching sequence (ROUGE-L), ensuring a comprehensive evaluation of the text generation quality. For accuracy, F1, ROUGE-1 and ROUGE-L, their higher values reflect the better performance. For MAE and RMSE, their lower value represent the better performance. Additionally, we use accuracy to measure the MIPS performance (MIPS accuracy), representing the ratio of MIPS results under device variation and MIPS results without device variation (references).

4.1.4 Baselines. As this is the first work to improve the RAG robustness on Edge-based CiM, we do not have state-of-the-art for comparison. As such, we construct baselines from the past noise mitigation methods originally designed to boost DNN robustness. The first baseline is selective write verify [21] (SWV). While it originally utilizes the second derivation to evaluate the device variation impact on neural network weights, we use the second derivation to measure the embedding deviation between the ground truth embedding and the embedding under device variation. The second baseline is (CxDNN) [45]. While they use compensation factor to improve the robustness of vector-matrix multiplication, we use the compensation factor to calibrate the embedding impacted by device variation. The third baseline is CorrectNet [46], where it utilizes the cross entropy loss and regularization to improve the robustness of neural networks in CiM. To use it as a baseline, we also use the cross entropy loss regularization as the loss function to

calibrate the device output embedding. Additionally, we examine the **Vanilla RAG**, which contains no noise mitigation methods, as our fourth baseline. The baselines use the same experimental setting as our framework does.

4.2 Results

For RAG, it can be simplified as the combination of MIPS and LLM, where the MIPS as a retriever searches the appropriate information and the LLM as a generator processes the searched results. Hence, in our experiments, we first evaluate the performance of MIPS under the device variation of device-1. We take the MIPS results obtained without device variation as the references (*i.e.*, ground truth). Using the metric of MIPS accuracy, we examine how many MIPS results under device variation will match the references. Since the quality of retrieved content largely depends on the base sentence embedding model, and we focus on mitigating the device variation impact on the embedding model, we do not assess the quality of references.

As shown in Table 3, our framework using the two data construction methods outperforms the four baselines across five datasets. It shows that our framework can mitigate the embedding perturbation due to device variation. These results can also correspond to the preliminary study shown in Figure 2, where the increment of σ in naive Gaussian noise will jeopardize the MIPS performance.

Table 3: Performance (MIPS accuracy) comparison between our framework and baselines. Accuracy is computed based on MIPS-retrieved documents under device variation of device-1 and the these retrieved without device variation.

Dataset	Citation	Movie	Rating	News	DBLP
SWV	0.4200	0.1728	0.1050	0.0855	0.2295
CxDNN	0.4401	0.2017	0.0503	0.0754	0.1681
CorrectNet	0.4013	0.0699	0.0509	0.0533	0.1609
Vanilla RAG	0.4547	0.1694	0.0933	0.0649	0.1747
RoCR-CDE	0.9231	0.4639	0.1583	0.1921	0.2750
RoCR-CDI	0.9344	0.4355	0.1266	0.1708	0.2905

After we compare the MIPS performance of our framework and baselines, we further present a comprehensive evaluation to show the RAG performance of them. We use Gemma-2B as the LLM in RAG. Additionally, with Gemma-2B, we run RAG without device variation to observe its ideal performance, where we get 0.5200 of accuracy for Citation, 0.3728 of accuracy for Movie, 0.3150 of MAE for Rating, 0.0855 of ROUGE-1 for News, and 0.2295 of ROUGE-1 for DBLP. On five CiM devices, whose device variations have been shown in Table 2, we examine RAG with five datasets. As shown in Table 1, given the same datasets, it is clear that each device variation significantly compromises the RAG robustness, whereas our framework can mitigate the different device variation. For example, the RAG performance for Citation dataset on Device-2 can range from 0.18 to 0.48, while our framework can boost the accuracy performance of Citation dataset above 0.5 for all five devices. Compared to the four baselines whose performances are relatively worse than the ideal performance, our framework significantly approaches and sometimes outperforms the ideal performance via generating better sentence embeddings. This is because RoCR also serves as a regularization to improve the model’s generalization.

In addition, we evaluate the impact of different LLMs on the performance of our framework. As Figure 1 shown, the LLM takes the concatenation of MIPS searched data and user query as the input and generates the response regarding the user query. Since different LLMs may have different response given the same query, we select four emerging edge-friendly medium-size LLMs in our experiments to examine the performance of our framework. Gemma-2B [47] is a new SOTA open model introduced by Google, with 4.95G model weights. According to Google, Gemma can outperform the same sized Llama-2 in reasoning capabilities. Hence, we also use Llama-2-3B [48], one of the earliest open LLMs introduced by Meta, with 6.85G model weights. Similarly, Phi-2 [49] released by Microsoft, is a powerful small LLM with 5G model weights. Additionally, Mistral-7B-GPTQ [50] made by Mistral AI, is a well-performed LLM after Llama model. We select dataset *Citation* and dataset *Moive*. We use the default experimental setting with $\sigma = 0.1$ and use CiM Device-1 as the experimental environment. The results are shown on Figure 6. It is evident that our framework outperforms each baseline across five CiM devices. Besides, the performance of each baseline on the same dataset can be largely different given different device, while our framework can produce a more robust performance.

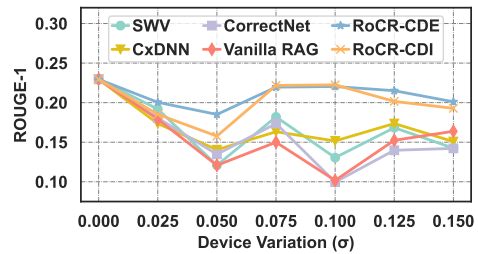


Figure 7: Performance comparison between our framework and four baselines on CiM device-1 with different device variation σ , given dataset DBLP.

By default, we use $\sigma = 0.1$ to calculate the device variation of the five CiM devices. We also conduct an additional study to evaluate our framework given different σ values. Since we have already use dataset Citation and dataset Movie to study the performance of our frameworks seen in Figure 6, we choose a different dataset DBLP, using ROUGE-1 as the metric. For the LLM in RAG, we choose Mistral-7B. We examine the σ values higher and lower than 0.1, including 0, 0.025, 0.05, 0.075, 0.125, and 0.15. The case of $\sigma = 0$ reflects the ideal performance. For the CiM device, we use CiM device-1. As shown in Figure 7, our framework outperforms baselines across different device variation values.

Finally, RoCR is a training method that generates more robust weights for the sentence embedding model. It does not change the model structure. Thus, there is no hardware (*e.g.*, energy and latency) overhead during inference.

5 CONCLUSION

In this paper, we present a novel framework for retrieval-augmented generation (RAG) acceleration via computing-in-memory (CiM) architectures. Our approach provide a solution to free RAG from

the constraints of latency and scalability on edge devices. By optimizing the sentence embedding model, our framework enable the utilization of CiM devices in storing and processing the document embeddings, minimizing the impact of CiM device variations. Experimental results show that our framework achieves superior RAG performance and largely mitigates the impact of device variations. This paper marks the first RAG acceleration via CiM framework.

REFERENCES

- [1] Marialena Bevilacqua, Kezia Oketch, Ruiyang Qin, Will Stamey, Xinyuan Zhang, Yi Gan, Kai Yang, and Ahmed Abbasi. When automated assessment meets automated content generation: Examining text quality in the era of gpts. *arXiv preprint arXiv:2309.14488*, 2023.
- [2] Ruiyang Qin, Yuting Hu, Zheyu Yan, Jinjun Xiong, Ahmed Abbasi, and Yiyu Shi. Fl-nas: Towards fairness of nas for resource constrained devices via large language models. *arXiv preprint arXiv:2402.06696*, 2024.
- [3] Seth Neel and Peter Chang. Privacy issues in large language models: A survey, 2023.
- [4] Karabacak et al. Embracing large language models for medical applications: Opportunities and challenges. *Cureus*, May 2023.
- [5] Xu et al. Can large language models be good companions? an llm-based eyewear system with conversational common ground, 2023.
- [6] Li et al. Personal llm agents: Insights and survey about the capability, efficiency and security, 2024.
- [7] Ruiyang Qin, Jun Xia, Zhengze Jia, Meng Jiang, Ahmed Abbasi, Peipei Zhou, Jingtong Hu, and Yiyu Shi. Enabling on-device large language model personalization with self-supervised data selection and synthesis. *arXiv preprint arXiv:2311.12275*, 2023.
- [8] Frantar et al. Gptq: Accurate post-training quantization for generative pre-trained transformers. *arXiv preprint arXiv:2210.17323*, 2022.
- [9] Ligeng Zhu, Lanxiang Hu, Ji Lin, Wei-Ming Chen, Wei-Chen Wang, Chuang Gan, and Song Han. Pockengine: Sparse and efficient fine-tuning in a pocket. In *Proceedings of the 56th Annual IEEE/ACM International Symposium on Microarchitecture*, pages 1381–1394, 2023.
- [10] Lewis et al. Retrieval-augmented generation for knowledge-intensive nlp tasks. *Advances in Neural Information Processing Systems*, 33:9459–9474, 2020.
- [11] Hu et al. Lora: Low-rank adaptation of large language models. *arXiv preprint arXiv:2106.09685*, 2021.
- [12] Kang et al. Enabling cost-effective data processing with smart ssd. In *2013 IEEE 29th symposium on mass storage systems and technologies (MSST)*. IEEE, 2013.
- [13] BanaGozar et al. Cim-sim: computation in memory simulator. In *Proceedings of the 22nd International Workshop on Software and Compilers for Embedded Systems*.
- [14] Sze et al. Efficient processing of deep neural networks: A tutorial and survey. *Proceedings of the IEEE*, 105(12):2295–2329, 2017.
- [15] Peng et al. Dnn+ neurosim: An end-to-end benchmarking framework for compute-in-memory accelerators with versatile device technologies. In *2019 IEEE international electron devices meeting (IEDM)*, pages 32–5. IEEE, 2019.
- [16] Chen et al. Eyeriss: A spatial architecture for energy-efficient dataflow for convolutional neural networks. *ACM SIGARCH computer architecture news*, 44(3):367–379, 2016.
- [17] Yan et al. Compute-in-memory based neural network accelerators for safety-critical systems: Worst-case scenarios and protections. *IEEE Transactions on Computer-Aided Design of Integrated Circuits and Systems*, 2024.
- [18] Jeong et al. Variation-tolerant and low r-ratio compute-in-memory rram macro with capacitive ternary mac operation. *IEEE Transactions on Circuits and Systems I: Regular Papers*, 2022.
- [19] Jiang et al. Device-circuit-architecture co-exploration for computing-in-memory neural accelerators. *IEEE Transactions on Computers*, 70(4):595–605, 2020.
- [20] Feinberg et al. Making memristive neural network accelerators reliable. In *2018 IEEE International Symposium on High Performance Computer Architecture (HPCA)*, pages 52–65. IEEE, 2018.
- [21] Yan et al. Swim: Selective write-verify for computing-in-memory neural accelerators. In *2022 59th ACM/IEEE Design Automation Conference (DAC)*. IEEE, 2022.
- [22] Yan et al. Uncertainty modeling of emerging device based computing-in-memory neural accelerators with application to neural architecture search. In *2021 26th Asia and South Pacific Design Automation Conference (ASP-DAC)*. IEEE, 2021.
- [23] Gao et al. Bayesian inference based robust computing on memristor crossbar. In *2021 58th ACM/IEEE Design Automation Conference (DAC)*. IEEE, 2021.
- [24] Yan et al. Improving realistic worst-case performance of nvcim dnn accelerators through training with right-censored gaussian noise. *2023 International Conference on Computer-Aided Design (ICCAD)*, 2023.
- [25] Mengyuan Li, Ann Franchesca Laguna, Dayane Reis, Xunzhao Yin, Michael Niemier, and X Sharon Hu. Imars: An in-memory-computing architecture for recommendation systems. In *Proceedings of the 59th ACM/IEEE Design Automation Conference*, pages 463–468, 2022.
- [26] Shim et al. Two-step write-verify scheme and impact of the read noise in multilevel rram-based inference engine. *Semiconductor Science and Technology*.
- [27] Yao et al. Fully hardware-implemented memristor convolutional neural network. *Nature*, 577(7792):641–646, 2020.
- [28] Shin et al. Fault-free: A fault-resilient deep neural network accelerator based on realistic rram devices. In *2021 58th ACM/IEEE Design Automation Conference (DAC)*. IEEE, 2021.
- [29] Chen et al. A simple framework for contrastive learning of visual representations. In *International conference on machine learning*, pages 1597–1607. PMLR, 2020.
- [30] Weinberger et al. Distance metric learning for large margin nearest neighbor classification. *Advances in neural information processing systems*, 18, 2005.
- [31] Dewen Zeng, Yawen Wu, Xinrong Hu, Xiaowei Xu, Haiyun Yuan, Meiping Huang, Jian Zhuang, Jingtong Hu, and Yiyu Shi. Positional contrastive learning for volumetric medical image segmentation. In *Medical Image Computing and Computer Assisted Intervention—MICCAI 2021: 24th International Conference, Strasbourg, France, September 27–October 1, 2021, Proceedings, Part II 24*, pages 221–230. Springer, 2021.
- [32] Gao et al. Simcse: Simple contrastive learning of sentence embeddings. *arXiv preprint arXiv:2104.08821*, 2021.
- [33] Zur et al. Noise injection for training artificial neural networks: A comparison with weight decay and early stopping. *Medical physics*, 36(10):4810–4818, 2009.
- [34] Malireddy et al. Scar: Sentence compression using autoencoders for reconstruction. In *Proceedings of the 58th Annual Meeting of the Association for Computational Linguistics: Student Research Workshop*, pages 88–94, 2020.
- [35] Salemi et al. Lamp: When large language models meet personalization. *arXiv preprint arXiv:2304.11406*, 2023.
- [36] F Maxwell Harper and Joseph A Konstan. The movielens datasets: History and context. *Acm transactions on interactive intelligent systems (tiis)*, 5(4):1–19, 2015.
- [37] Ni et al. Justifying recommendations using distantly-labeled reviews and fine-grained aspects. In *EMNLP-IJCNLP*, pages 188–197, 2019.
- [38] Rishabh Misra. News category dataset. *arXiv preprint arXiv:2209.11429*, 2022.
- [39] Tang et al. Arnetminer: extraction and mining of academic social networks. In *Proceedings of the 14th ACM SIGKDD international conference on Knowledge discovery and data mining*, pages 990–998, 2008.
- [40] Hugging Face. Sentence transformers: all-minilm-l6-v2. <https://huggingface.co/sentence-transformers/all-MiniLM-L6-v2>.
- [41] Liu et al. Architecture-circuit-technology co-optimization for resistive random access memory-based computation-in-memory chips. *Science China Information Sciences*, 66(10):200408, 2023.
- [42] Wei et al. Switching pathway-dependent strain-effects on the ferroelectric properties and structural deformations in orthorhombic hfo2. *Journal of Applied Physics*, 131(15), 2022.
- [43] Chai et al. Root mean square error (rmse) or mean absolute error (mae)?—arguments against avoiding rmse in the literature. *Geoscientific model development*, 7(3):1247–1250, 2014.
- [44] Chin-Yew Lin. Rouge: A package for automatic evaluation of summaries. In *Text summarization branches out*, pages 74–81, 2004.
- [45] Jain et al. Cxdnn: Hardware-software compensation methods for deep neural networks on resistive crossbar systems. *ACM Transactions on Embedded Computing Systems (TECS)*, 18(6):1–23, 2019.
- [46] Eldebiky et al. Correctnet: Robustness enhancement of analog in-memory computing for neural networks by error suppression and compensation. In *2023 Design, Automation & Test in Europe Conference & Exhibition (DATE)*. IEEE, 2023.
- [47] Gemma Team. Gemma: Open models based on gemini research and technology. *arXiv preprint arXiv:2403.08295*, 2024.
- [48] Geng et al. Openllama: An open reproduction of llama, 2023.
- [49] Gunasekar et al. Textbooks are all you need. *arXiv preprint arXiv:2306.11644*, 2023.
- [50] Jiang et al. Mistral 7b. *arXiv preprint arXiv:2310.06825*, 2023.